TuEngr Group

International Transaction Journal of Engineering, Management, & Applied Sciences & Technologies

http://TuEngr.com

MICRO-HARDNESS PROFILE AND MICROSTRUCTURE CHARACTERIZATION IN FRICTION-STIR-PROCESSING ZONE OF THE ZrO_2/CNT NANO-COATED ST37 STEEL

Seyed Mohammad Hossein Sharifi [a*], Armin Sabetghadam-Isfahani [a]

[a] *Department of Mechanical Engineering, Petroleum University of Technology (PUT), Ahvaz Faculty, IRAN*

ARTICLEINFO

Article history:
Received 14 December 2018
Received in revised form 15 March 2019
Accepted 19 March 2019
Available online
19 March 2019

Keywords:
Metal Fabrication; SZ; TMAZ; HAZ Phases; Zener Pinning Effect; Zirconium dioxide; Nano-coating Dispersing; Diamond Pyramid Hardness.

ABSTRACT

The effect comparison of applying Friction Stir Processing (FSP) with two different Nanoparticles; CNT (Carbon Nano Tubes) and ZrO_2, on St37 steel Micro-hardness changes has been investigated. In FSP fabrication method, the rotational speed was 900 rpm and the traverse speed was 100 mm/min. The obtained Micro-hardness results from both Nano-particles have been compared with the one in Base Metal (BM). Both Nanoparticles (CNT and ZrO_2) were tested in the same total dominant condition. It is note-able that the nugget zones' Micro-hardness of both FSP Nano-coated samples have experienced a great promotion in comparison to the one in BM. However, the CNT one allocates a greater promotion slope to itself. By comparing the three fabrication zone products (Nugget Zone, TMAZ, HAZ); it will be understood that CNT sample experiences a greater difference between three fabrication zones rather than the ZrO_2 ones.

1. INTRODUCTION

St37 steel has been widely used in the construction of pipelines in the petroleum and gas industries. Micro-hardness is one of the key determinant factors in designing pipelines and weld metals. Recently, Micro-hardness has been extensively used in order to improve the mechanical properties of steels and weld metals. Mechanical property enhancements can be achieved using the refinement of microstructures. Factors such as dispersion of active nucleation sites, austenite grain size, and cooling have great influence of formation of acicular ferrite [1-8].

Several types of ferrite structures may be encountered while studying the microstructure of weld metals; including grain boundary allotriomorphic ferrite, polygonal ferrite, Widmanstätten ferrite, and acicular ferrite. Allotriomorphic ferrite grows from columnar

*Corresponding author (Seyed Mohammad Hossein Sharifi) E-mail: sharifi@put.ac.ir Volume 10 No.4 ISSN 2228-9860 eISSN 1906-9642 http://TUENGR.COM/V10/477.pdf DOI: 10.14456/ITJEMAST.2019.46

austenite grain boundaries and can sometimes be seen as almost continuous grain boundary layers with various thicknesses. Widmanstätten ferrite nucleates grow from the grain boundary allotriomorphic ferrite layers or austenite grain boundaries and develop into austenite grains in the form of thin wedge-shaped laths. Basically, there is a difference in nucleation between acicular ferrite and bainite that formed at the same temperature range and transformation mechanism. The fine interlocking microstructure of acicular ferrite nucleates intergranular in the form of separate laths from non-metallic inclusions within large austenite grains, whereas the bundle morphology of bainite grows at small austenite grains or austenite grain boundaries, forming sheaves of parallel laths [9, 10].

Weld metals show the best combination of strength and impact toughness in intergranular acicular ferrite since density is increased in high-angled boundaries. Boundaries have different crystallographic orientation, therefore, they act like strong barriers and change crack growth direction [10-12]. In the two past few decades, the effectiveness of various non-metallic inclusions in producing intergranular ferrite in low alloy steels and weld metals has been investigated. Several factors, including the chemical composition, shape, size and distribution of inclusions, have strongly influenced the potential nucleation sites for the formation of intergranular ferrite [1, 2, 4-7, 13-19].
One of the newly introduced methods for microstructure refinement is a solid-state process called Friction Stir Processing (FSP) which uses the same approach as the Friction Stir Welding [20, 21]. In FSP, as a result of friction between the rotating tool and underlying substrate, the localized heating increases the local temperature of workpiece to a range that plastic deformation can occur and fine grains are resulted [20]. Substrate plastic deformation and interaction between nanoparticles are limited due to the process temperature which is well below the melting point of the workpiece. Thus, grain refinement and fabricating composite with FSP method is very attractive. Another approach of microstructure refinement is Nano-coating with an electrode, in which mechanical properties and microstructure of weld metals are enhanced by adding nanoparticles to conventional electrodes. For instance, adding nanoparticles such as TiO [6, 19], TiO2 [22, 23], and Ti2O3 [2, 13, 15] to low alloy steels and weld metals have positive effects on nucleating intergranular ferrite. Present investigation compares the results from applying FSP method with ZrO2 nanoparticles on the improvement of micro-hardness in Stir Zone (SZ), Heat Affected Zone (HAZ) and Thermo-Mechanic Affected Zone (TMAZ) with similar results from Nano-coating method in the columnar zone and reheated zone [24].

2. EXPERIMENTAL DETAILS

2.1 HARDNESS AND MICRO-HARDNESS

Hardness is a material property that enables it to resist against plastic deformation, usually by penetration. Measuring the hardness in Microscale, presents the Micro-hardness. There are two common methods for measuring the Micro-hardness; Vickers/DPH (Diamond Pyramid Hardness) and KNOOP. In this paper, Vickers has been used. The Vickers

hardness test method (or DPH) consists of indenting the test material using a diamond indenter. It forms the material into a right pyramid with a square base and an angle of 136 degrees between opposite faces. The material is then subjected to a load ranging between 1 to 100 KgF; the full load is applied for 10 to 15 seconds. Afterward, when the load is removed, the two diagonals of the indentation left in the surface of the material are measured by a microscope and their average is calculated; the area of the sloping surface of the indentation is also calculated. The Vickers hardness is the quotient obtained by dividing the applied KgF load by the square millimeters area of the indentation.

2.2 MATERIAL PHASE (AUSTENITE, FERRITE, PEARLITE)

A comparison between material phases shows that in the austenite phase, grain boundaries can be recognized and the grain size is finer. In Ferrite phase, the grain size is finer and more regular than pearlite phase; grain boundaries, however, are not as recognizable as in austenite phase. Pearlite phase has structural turbidity and grain boundaries are not recognizable too. So as it is clear, having a region in austenite phase is much better than other phases; since the grain sizes are more recognizable, grains are more regular, and the form of grains is more homogeneous. All used Base Metals (BMs) in these experiments were in Ferrite or Pearlite phases that is a negative point for samples and changing their phases by a process to austenite is a great benefit for the process. Concluded from the results that the chief advantage of the FSP method is gradually converting the BM's phase from pearlite or ferrite to austenite in four steps as shown in Figure 1.

2.3 FRICTION STIR PROCESSING (FSP)

FSP is a solid-state process for the joining and processing of different materials. The process of friction stirring involves a cylindrical tool with a shoulder and a projecting pin. The tool is spun at pre-determined revolutions per minute (RPM) and then plunged into the material and traversed across it. Friction stir processing can be done on a single sheet of material to change the mechanical properties by changing the microstructure. For FSP, plates can be abutted and joined by traversing the tool along the seam line. An anvil is placed under the material to react to the plunge force. As the tool traverses along the weld line, the material undergoes severe plastic deformation under adiabatic conditions and is simultaneously heated via frictional and adiabatic dissipation. Figure 2, illustrates the basic FSP nomenclature.

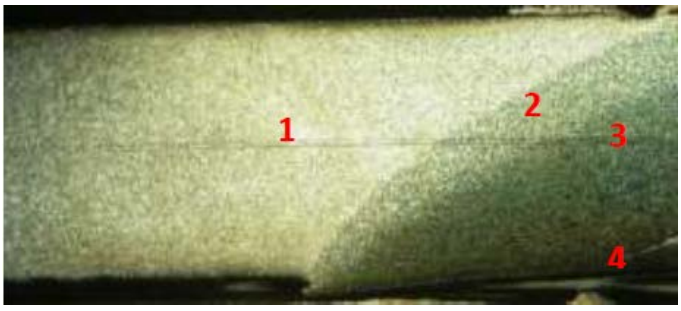

Figure 1: The conversion of the base metal into the austenite phase in four steps: 1) BM, 2) HAZ, 3) TMAZ, 4) SZ.

*Corresponding author (Seyed Mohammad Hossein Sharifi) E-mail: sharifi@put.ac.ir Volume 10 No.4 ISSN 2228-9860 eISSN 1906-9642 http://TUENGR.COM/V10/477.pdf DOI: 10.14456/ITJEMAST.2019.46

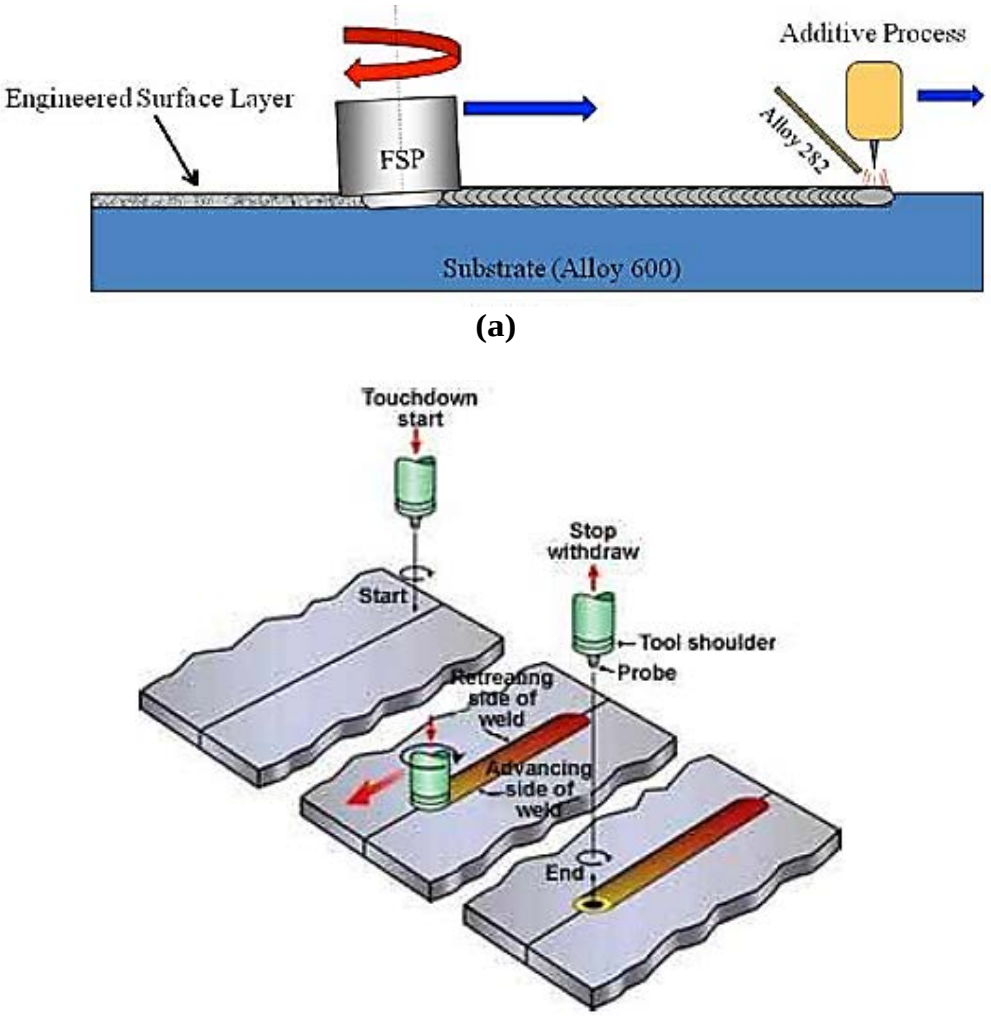

Figure 2: FSP Nomenclature; (a) Front View, (b) 3D View [4].

2.4 ZONES IN FSP NANO-COATING METHOD

There are three main produced zones in the workpiece after applying the FSP method on it; these zones are named Stir Zone (SZ), Heat Affected Zone (HAZ), and Thermal and Mechanical Affected Zone (TMAZ). As it is clear from the zones' names, SZ is a region where the maximum value of the Nanoparticle is dispersed in it, and totally, the whole characteristics of the BM are changed both from point of mechanical and thermal view. These characteristics changes are perceptible in Micro and Macro scale. The second zone TMAZ is a region where Nanoparticle is dispersed in it but not as much as SZ. In this region, the driving force of dispersion is combined from mechanical forces (caused by the pin traverse and rotational motion) and the thermal effects (caused by the friction). The third zone HAZ is a region where its Nanoparticle is a little bit less than the TMAZ. In this region, the driving force of dispersion is only caused by thermal effects. The Stir Zone (SZ) is the most noteworthy zone in the workpiece because unlike the other two segments, Nano dispersion occurs mainly at this zone. Nanodispersion in all three mentioned zones are shown in Figure 1.

2.5 CHEMICAL COMPOSITION

A 25.4mm by 25.4mm sample was sectioned from a corner of the plate using a Struers Sectom-10 diamond saw. This sample was sent for chemical analysis at Metallurgy Laboratory of Sharif Jahad, to determine the chemical composition of the steel used in this work. Table (1) gives the composition limits for St 37 steel according to MIL-S-16216K [29]. Chemical composition and mechanical properties of BM are presented in Table 1 and Table 2, respectively.

Table1: Chemical Composition of St37 Steel.

St 37	Fe	C	Si	Mn	P	S	Cr	Ni	Mo	Al
Magnitude	Base	0.131	0.0657	0.445	0.0092	0.0207	0.0278	0.0286	0.0023	0.0403
St 37	Co	Cu	Nb	Ti	V	W	Pb	Sn	As	Zr
Magnitude	0.0045	0.0616	0.00072	0.00046	0.0023	0.0049	0.0023	0.0043	0.0029	0.00054

Table 2: Tensile Results for the FSPed Specimens in 1 Pass.

	Nano Particle	E (GPa)	YTS (MPa)	Elongation (%)	Promotion Percentage YTS (%)
FSPed Sample	ZrO2	136	342	2.5	38.59
	CNT	172	430	2.5	51.16
Base Metal	-----	105	210	2.5	0.00

2.6 Procedure

Herein, the total procedure of the experiments is described which all had been done at room temperature. The BM used in this research was St37 steel of which chemical compositions and mechanical properties are listed in Tables 1 and 2, respectively.
First, in the FSP method four workpieces were provided with lengths, widths, and thicknesses of 200, 150 and 2 mm respectively. A groove was then made by wire cut in a straight line along the middle length of each workpiece. Afterward, ZrO_2 and CNT Nanoparticles with Aston were inserted into the groove; and finally, FSP process with a tool tilt angle of 3 degrees was done on the workpieces. The rotational and traverse speed were 900 rpm and 100 mm/min, respectively.

Second, in Nano-coating method, three St37 workpieces with dimensions of 300 (mm) × 276 (mm) × 2 (mm) were prepared. Third, a piece of FSPed samples including; BM, HAZ, TMAZ, and SZ were cut to undergo DPH test. The mechanism of the DPH is choosing 3 points from each region (BM, HAZ ...) and obtaining the average value of the hardness there. Then combining these obtained average values as a profile which is called Micro-hardness profile.

3. MICRO-HARDNESS TEST RESULTS AND DISCUSSION

The obtained Micro-hardness results of two different Nano-particles, namely ZrO_2 and CNT FSP Nano-coating are shown in Figure 3 and Figure 4 respectively; and eventually,

*Corresponding author (Seyed Mohammad Hossein Sharifi) E-mail: sharifi@put.ac.ir Volume 10 No.4 ISSN 2228-9860 eISSN 1906-9642 http://TUENGR.COM/V10/477.pdf DOI: 10.14456/ITJEMAST.2019.46

are compared with each other in Table 3. This promotion of Micro-hardness in FSP is caused by the process in which the microstructure of the workpiece changes from perlite (In BM) to austenite (In SZ). This change in microstructure results caused from Zener Pinning Effect (ZPE) which states that by decreasing the grain size of the particles, more energy is stored on the grain boundaries which produces more regular grains and smaller grain sizes. The bases of ZPE is measuring the effect of fine particles dispersion on the movement of low- and high angle grain boundaries through a polycrystalline material. Small particles act to prevent the motion of such boundaries by exerting a pinning pressure which counteracts the driving force pushing the boundaries. The mathematical description of the ZPE is so important. Figure 5 illustrates a boundary of energy γ per unit area where it intersects with an incoherent particle of radius r. The pinning force acts along the line of contact between the boundary and the particle i.e. a circle of diameter $AB = 2\pi r\, cos\theta$. The force per unit length of the boundary in contact is $\gamma\, sin\theta$. Hence, the total force acting on the particle-boundary interface is

$$F = 2\pi r\gamma\, cos\theta\, sin\theta \tag{1}.$$

The maximum restraining force occurs when $\theta = 45°$, and so

$$F_{max} = \pi r\gamma \tag{2}.$$

In order to determine the pinning force by a given dispersion of particles, Clarence Zener made several important assumptions [25]:

- The particles are spherical.
- The passage of the boundary does not alter particle-boundary interaction.
- Each particle exerts the maximum pinning force on the boundary regardless of the contact position.
- The contacts between particles and boundaries are completely random.
- The number density of particles on the boundary is that expected for a random distribution of particles.

For a volume fraction F_v of randomly distributed spherical particles of radius r, the number per unit volume (number density) is given by:

$$N_{\text{Total}} = \frac{3F_v}{4\pi r^3} \tag{3}.$$

Given the assumption that all particles apply the maximum pinning force, F_{max} the total pinning pressure exerted by the particle distribution per unit area of the boundary is

$$\text{Ps} = N_{\text{Interact}} F_{\text{max}} = \frac{3F_v\gamma}{2r} \tag{4}.$$

Only particles within one radius (solid circles) can intersect a planar boundary, Figure 6**.** This is referred to as the Zener pinning pressure. It results that large pinning pressures are produced by:

- Increasing the volume fraction of particles,
- Reducing the particle size.

The Zener pinning pressure is orientation dependent, which means that the exact pinning pressure depends on the amount of coherence at the grain boundaries [25].

According to Equations (1) and (2), the more spherical and homogenous grains, the more force on the grains' boundaries, and the more force on the grains' boundaries the more benefited composite.

As it is clear from Equations (3) and (4), the real magnitude of P_s cannot be calculated, but approximately can be observed. These approximate results are presented in Table 4. According to the results of Table 4, it can be concluded that the pressure on the CNT coated steel borders is more than the ZrO_2 one; so it produces smaller grains. Herein, the more benefited composite refers to *promoting* a metal from characteristics point of view by *an efficient technique* and using the *optimized level of special Nano-particles*. In this research, this benefited composite has been produced by FSP technique and an optimized level of ZrO_2 and CNT.

The microstructure of BM and SZ are shown in Figure 7. As it is observed, in FSP the greatest amount of Micro-hardness belongs to SZ and then reduces gradually by passing from HAZ to TMAZ and BM, respectively.

It is noteworthy to mention that in the CNT FSP Nano-coating method, there is more promotion in the microstructure of the workpiece, Figure 8. This happens because of the more homogeneous distribution of Nano CNT particles, and consequently, having more boundary energy and more homogeneous grain sizes. According to ZPE, having less homogeneous grain sizes shows fewer grain boundaries' energy. Therefore, there is more irregularity in grain sizes which prevents microstructure changings, namely ZrO_2 in comparison to CNT.

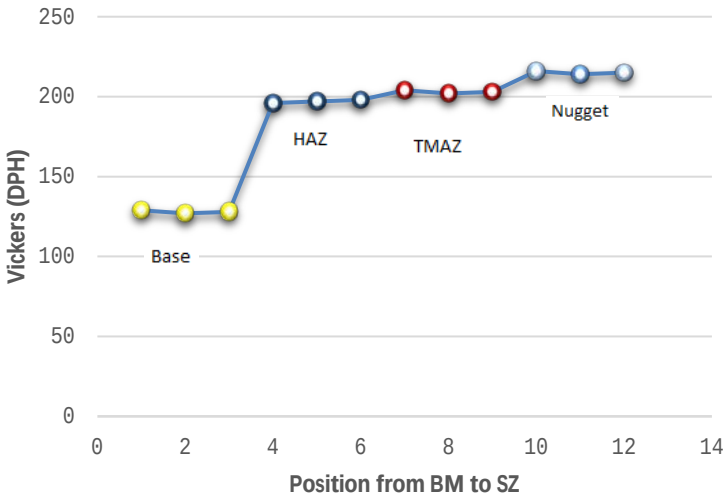

Figure 3: Micro-hardness profile in four different parts for ZrO_2.

Table 3: Comparison of Obtained Micro-hardness Results from Two Different Nanoparticles.

NanoParticle		Micro-hardness			
		BM	HAZ	TMAZ	SZ
Nano-coating	ZrO_2	128	197	203	215
	CNT	128	155	174	412

Table 4: The Zener Pinning Pressure for CNT and ZrO2 Coated BMs.

Particle	P_s
CNT	0.35 $F_v\gamma$
ZrO2	0.20 $F_v\gamma$

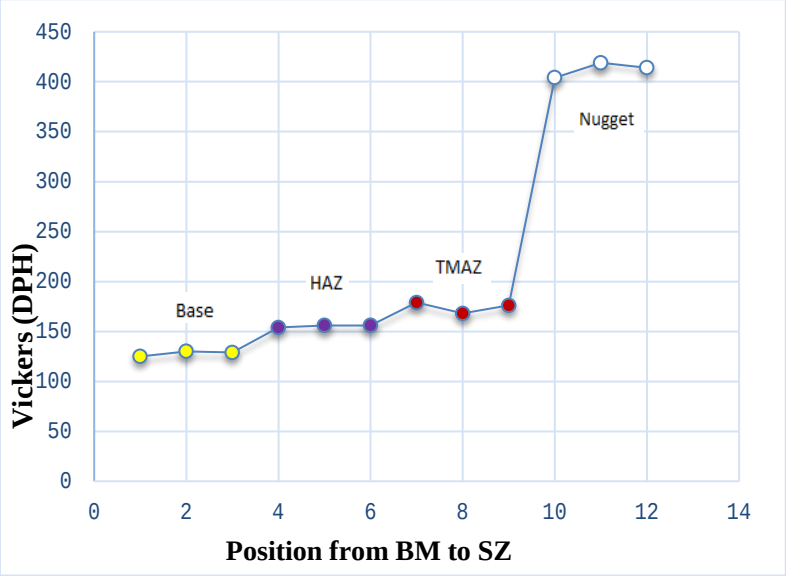

Figure 4: Micro-hardness profile in four different parts for CNT.

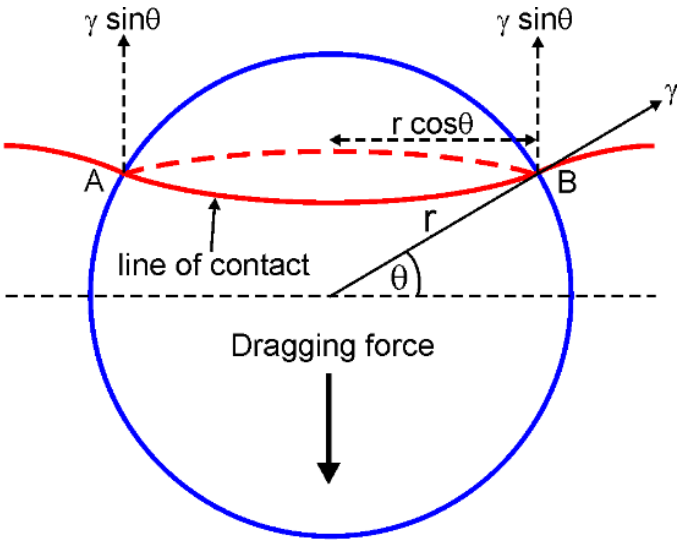

Figure 5: Schematic of the interaction a boundary and a particle [25].

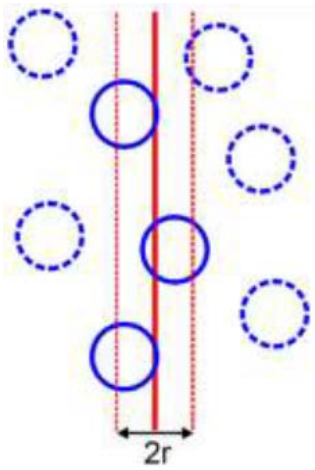

Figure 6: Only particles within one radius (solid circles) can intersect a planar boundary [25].

St37 BM hardness value was reported 128 on the diamond pyramid hardness scale (DPH). The variance between BM and the other three zones (SZ, HAZ, and TMAZ) is due to the non-homogenous nature of the material, including porosity and inclusion stringers. The results form martensitic microstructures produced by FSP show by approaching the TMAZ in the dry FSP microstructure, there is a gradual increase in hardness that peaks; it must be mentioned that the rate at which the hardness increases is at its greatest value in HAZ for ZrO_2 and in SZ for CNT, but the maximum hardness value occurs in SZ. For

instance, the increase of hardness for ZrO_2 from BM to HAZ is much more than its changes in TMAZ to SZ; but, for CNT, the hardness changes from TMAZ to SZ is in its maximum magnitude, and totally, the highest value of Micro-hardness is for SZ of CNT.

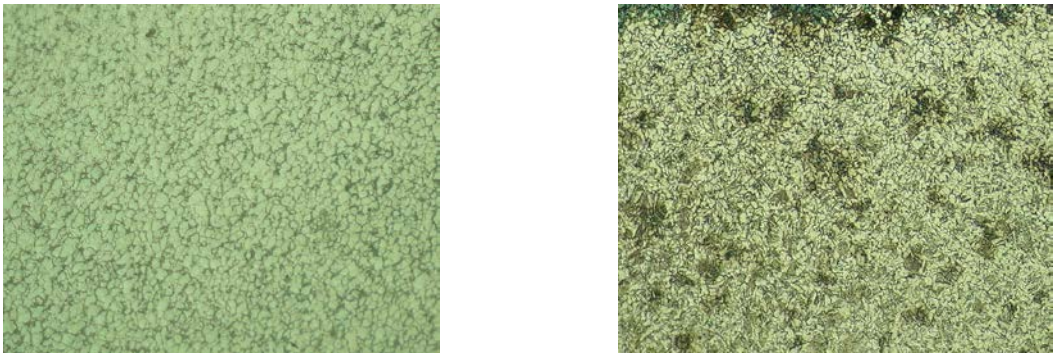

(a) (b)

Figure 7: (a) SZ of ZrO_2 FSPed Metal (100x), (b) BM (100x).

The hardness reaches its maximum and stays constant across the stir nugget –which also refers to SZ. Upon reaching the TMAZ, the hardness gradually decreases until the microstructure reaches the BM, Figures 3 and 4. This is attributed to its greater hardness value achieved by uniform dispersion of hard ceramic ZrO_2 and CNT reinforcements. Extra contribution goes to severe plastic deformation that promoted grain refinement by dynamic recrystallization process.

4. CONCLUSION

In this paper, the effect of applying FSP with two different Nanoparticles; CNT (Carbon Nano Tubes) and ZrO_2, on St37 steel Micro-hardness changes has been investigated. In the present FSP fabrication method, the rotational speed and traverse speed were considered 900 rpm and 100 mm/min, respectively. Both Nanoparticles (CNT and ZrO_2) were tested in the same total dominant condition. Micro-hardness profile was obtained for both Nano-particles including the three main zones: SZ, TMAZ, and HAZ. The obtained Micro-hardness results have been compared with the one in BM. It is note-able that the Stir Zone's Micro-hardness of both FSP Nano-coated samples have experienced a great promotion in comparison to the one in BM. As it is clear in Table 3, for ZrO_2 coated sample, the Micro-hardness has promoted from 128 in BM to 215 in SZ, and for the CNT one, the Micro-hardness has promoted from 128 in BM to 412 in SZ. Obviously, the CNT one has allocated a greater promotion slope to itself. Accordingly, by comparing the produced three fabrication zones (Nugget Zone, TMAZ, HAZ); it will be understood that CNT sample, experiences a greater difference between three fabrication zones rather than the ZrO_2 ones. Moreover, the produced grain sizes in the material after the process are more homogeneous in CNT sample rather than the ZrO_2 one, and both show more regular grain boundaries than the BM, Figures 7 and 8. The differences between ZrO_2 and CNT FSP coated samples are:

- First, in the CNT FSP coating, SZ has a martensitic microstructure and more homogeneous grain sizes.
- Second, from Figures 3 and 4, it can be observed that in the FSP method, Micro-hardness values

have minor differences in SZ and TMAZ for ZrO_2 but not for CNT. In FSP Nano-coating method, however, there is drastically changes in hardness values as we move toward the reheated zone.

Eventually, it can be concluded that using the FSP fabrication method is an efficient way to promote the metal hardness.

5. REFERENCES

[1] Bose-Filho, W., A. Carvalho, and M. Strangwood, Effects of alloying elements on the microstructure and inclusion formation in HSLA multipass welds. Materials characterization, 2007. 58(1): p. 29-39.

[2] Byun, J.-S., et al., Inoculated acicular ferrite microstructure and mechanical properties. Materials Science and Engineering: A, 2001. 319: p. 326-331.

[3] Calcagnotto, M., D. Ponge, and D. Raabe, Effect of grain refinement to 1μm on strength and toughness of dual-phase steels. Materials Science and Engineering: A, 2010. 527(29): p. 7832-7840.

[4] Court, S.A. and G. Pollard, Inclusion chemistry and morphology in shielded metal arc (SMA) steel weld deposits. Metallography, 1989. 22(3): p. 219-243.

[5] Pan, T., et al., Kinetics and mechanisms of intragranular ferrite nucleation on non-metallic inclusions in low carbon steels. Materials Science and Engineering: A, 2006. 438: p. 1128-1132.

[6] St-Laurent, S. and G. L'Espérance, Effects of chemistry, density and size distribution of inclusions on the nucleation of acicular ferrite of C□Mn steel shielded -metal-arc-welding weldments. Materials Science and Engineering: A, 1992. 149(2): p. 203-216.

[7] Terashima, S. and H. Bhadeshia, Size distribution of oxides and toughness of steel weld metals. Science and Technology of Welding & Joining, 2006. 11(5): p. 580-582.

[8] Wang, C., et al., Effect of microstructural refinement on the toughness of low carbon martensitic steel. Scripta Materialia, 2008. 58(6): p. 492-495.

[9] Babu, S.S., The mechanism of acicular ferrite in weld deposits. Current opinion in Solid state and Materials Science, 2004. 8(3): p. 267-278.

[10] Bhadeshia, H., Bainite in steels: transformation, microstructure and properties. IOM Communications, London, 2001: p. 237-276.

[11] Diaz-Fuentes, M., A. Iza-Mendia, and I. Gutierrez, Analysis of different acicular ferrite microstructures in low-carbon steels by electron backscattered diffraction. Study of their toughness behavior. Metallurgical and Materials Transactions A, 2003. 34(11): p. 2505-2516.

[12] Flower, H. and T. Lindley, Electron backscattering diffraction study of acicular ferrite, bainite, and martensite steel microstructures. Materials Science and Technology, 2000. 16(1): p. 26-40.

[13] Byun, J.-S., J.-H. Shim, and Y.W. Cho, Influence of Mn on microstructural evolution in Ti-killed C–Mn steel. Scripta materialia, 2003. 48(4): p. 449-454.

[14] M.D. Fuentes, I.M., I. Gutiérrez, Materials Science Forum, 1998: p. 245–252.

[15] Peng, Y., W. Chen, and Z. Xu, Study of high toughness ferrite wire for submerged arc welding of pipeline steel. Materials characterization, 2001. 47(1): p. 67-73.

[16] Shim, J.-H., et al., Nucleation of intragranular ferrite at Ti 2 O 3 particle in low carbon steel. Acta Materialia, 1999. 47(9): p. 2751-2760.

[17] Shim, J.-H., et al., Ferrite nucleation potency of non-metallic inclusions in medium carbon steels. Acta Materialia, 2001. 49(12): p. 2115-2122.

[18] Wu, K., Three-dimensional analysis of acicular ferrite in a low-carbon steel containing titanium. Scripta materialia, 2006. 54(4): p. 569-574.

[19] Zhang, D., H. Terasaki, and Y.-i. Komizo, In situ observation of the formation of intragranular acicular ferrite at non-metallic inclusions in C–Mn steel. Acta materialia, 2010. 58(4): p. 1369-1378.

[20] Ma, Z., Friction stir processing technology: a review. Metallurgical and Materials Transactions A, 2008. 39(3): p. 642-658.

[21] Mishra, R.S. and Z. Ma, Friction stir welding and processing. Materials Science and Engineering: R: Reports, 2005. 50(1): p. 1-78.

[22] Kiviö, M., L. Holappa, and T. Iung, Addition of dispersoid titanium oxide inclusions in steel and their influence on grain refinement. Metallurgical and Materials Transactions B, 2010. 41(6): p. 1194-1204.

[23] Nedjad, S.H. and A. Farzaneh, Formation of fine intragranular ferrite in cast plain carbon steel inoculated by titanium oxide nanopowder. Scripta Materialia, 2007. 57(10): p. 937-940.

[24] Fattahi, M., et al., Improvement of impact toughness of AWS E6010 weld metal by adding TiO 2 nanoparticles to the electrode coating. Materials Science and Engineering: A, 2011. 528(27): p. 8031-8039.

[25] Koch, C.C., Scattergood, R.O., Darling, K.A. and Semones, J.E., Stabilization of nanocrystalline grain sizes by solute additions. Journal of Materials Science: 2008, 43: 7264-7272.

Dr.Seyed Mohammad Hossein Sharifi is an Assistant Professor at Department of Mechanical Engineering, Petroleum University of Technology (PUT), Ahvaz Faculty, IRAN. His research encompasses Experiments, Numerical Simulations, Fatigue and Fracture Analysis, Friction Stir Processing Field with different Nano-particles, different Mechanical and Metallurgical Tests.

Armin Sabetghadam-Isfahani has an MSc degree in Applied Mechanics from the Petroleum University of Technology, Iran, Ahwaz. His researches are foam-filled thin-walled structures, modern and efficient fabrication methods. His work involves experiments, simulations, and math analyses on Friction Stir Processing Field, with different Nano-particles, different mechanical and metallurgical tests, under different operational conditions

*Corresponding author (Seyed Mohammad Hossein Sharifi) E-mail: sharifi@put.ac.ir Volume 10 No.4 ISSN 2228-9860 eISSN 1906-9642 http://TUENGR.COM/V10/477.pdf DOI: 10.14456/ITJEMAST.2019.46